ELSEVIER

Catalysis Today 53 (1999) 225–243

CATALYSIS TODAY

www.elsevier.com/locate/cattod

The effect of fractal surface roughness on diffusion and reaction in porous catalysts – from fundamentals to practical applications

Marc-Olivier Coppens *

Delft Department of Chemical Technology, Delft University of Technology, Julianalaan 136, 2628 BL Delft, The Netherlands

Abstract

'Amorphous' porous catalysts and catalyst supports have a rough internal surface. Small-angle and wide-angle X-ray scattering results confirm the original but inconclusive suggestion from adsorption experiments that this surface is often fractal on molecular scales. Not only does this imply that the accessible surface area depends on the size of the molecules moving through the pores, but there also exists an accessibility distribution along the surface. Transport and reaction processes may therefore depend on surface roughness, in a way that can be quantified using fractal geometry.

The effect of fractal surface roughness on Knudsen diffusion is discussed. An analytical expression for the Knudsen diffusivity is derived and the residence time distribution of the molecules is obtained from Monte-Carlo simulations. The equations for diffusion and reaction in fractal pores and in porous catalysts with a fractal internal surface are given. Practical examples – vinyl acetate production and the catalytic reforming of naphtha – illustrate the significant influence of fractal roughness on product yields and distributions of industrial processes, from the microscale up to the observable reactor scale. This indicates how conversions and selectivities may be increased by modifying the catalyst surface morphology.

1. Introduction

Catalysis is a surface process: molecules react on the catalyst surface, so that a high specific surface area is usually desirable. The heterogeneous catalysts used in many chemical applications are therefore either porous materials themselves or they are produced as tiny particles with a diameter of a few nanometers that are deposited on a porous support such as alumina or silica. Crystalline zeolites are finding an increasing use, yet many common catalysts and catalyst supports are amorphous.

Despite the ethymological suggestion from the name 'amorphous' that these materials would be shapeless, experiments show that they may in fact contain an internal symmetry, that of statistical scale invariance of the internal surface. Section 2 will review some of the observations that led to conclude that this is the case: many porous catalysts have a fractal internal surface within a certain range of scales.

Just like the translational symmetry of zeolites allows to model physico-chemical phenomena within their pore network, the fractal nature of the surface of materials such as certain mesoporous silicas or aluminas may help to model the same phenomena within their pore space. Section 3 reviews diffusion and reaction in a single fractal pore, and illustrates the in-

* Tel.: +31-15-278-4399
E-mail address: m.o.coppens@stm.tudelft.nl (M.-O. Coppens)

0920-5861/99/$ – see front matter
PII: S0920-5861(99)00118-2

fluence of the fractal surface morphology on conversion with a practical example: the production of vinyl acetate from ethylene, acetic acid and oxygen in a pore of its Pd/Al_2O_3 catalyst.

Knudsen diffusion is often the limiting transport mechanism of gas molecules in mesoporous materials. Since it is a result of collisions of gas molecules with the pore walls, the effect of the walls' fractal roughness on Knudsen diffusion should be investigated. This research is reviewed in Section 4.

Finally, Section 5 studies the effect of surface roughness on the product distributions at the industrial reactor scale. Known equations for multicomponent diffusion and reaction within a catalyst pellet are used, yet the parameters reflect the influence of roughness on reaction rates and diffusivities. Simulations of an industrial unit for the catalytic reforming of naphtha show the fractal effects on partial pressure profiles within catalyst particles, on reactor profiles, and, ultimately, on the product distributions at the outlet. Consequences for catalyst design are briefly discussed.

As the title already indicates, this paper does not intend to review the vast literature on fractals and porous media [1–5], but rather focuses on one particular issue: improving models for diffusion and reaction in porous catalysts by including the influence of the fractal internal surface roughness, and illustrating the consequences on processes from the catalyst pore scale up to the scale of an industrial unit. Many interesting related problems exist, but cannot be discussed here. Examples include studies of diffusion and reaction on Bethe lattices, percolation clusters and pore networks close to a percolation threshold [6–16]. Especially useful to design new types of catalysts is the problem of diffusion and reaction in a fractal pore tree [17–22] or on a fractal network [23–28], because such studies reveal qualitative deviations from the classical behavior seen in most existing catalysts. Also diffusion toward and reaction on the surface of fractal aggregates has been studied [18–20,29–35] as well as diffusion and reaction in the pore space of fractal materials [31,36–38].

Shortly, the pore space, the catalyst surface or the catalyst itself may be fractal and each of these assumptions leads to different laws. Rocks and other cracked materials may have a fractal pore network [3]; physiological networks such as a lung may be modeled as a fractal pore tree [39]; (aero)gels often have a fractal structure [1,40]. Transport and reaction through their pore networks is an important problem. Only a fractal surface is considered here, the most frequently observed case for what are commonly called 'amorphous' catalysts and supports [41,42].

2. Experimental study of the surface morphology of porous catalysts

The pore space within an amorphous porous solid is a labyrinth of narrow tortuous channels with rough walls. Electron microscopy images reveal a seemingly very irregular surface [10,43,44]. Digitizations of these images or imitations by randomly stacking spheres, cylinders or other shapes from Euclidean geometry have been used as models to study diffusion, flow and reaction by Monte-Carlo simulations [2,9,10,45–52]. Certain materials (e.g., certain silicas and titanias) do indeed consist of spherical aggregates, but most of them have entirely different morphologies. Until recently, possible nanometer-scale roughness was typically ignored, since no obvious way existed to model it in a simple yet realistic way. Also, the electron microscopy images used as a reference do not usually show such high resolutions. In most models roughness is altogether ignored and pores are simply represented by cylinders, spheres or other smooth shapes.

Most of the surface of a porous catalyst or support is internal. The specific accessible area is typically measured using nitrogen adsorption. Values found in this way are extremely high, e.g., 200 m^2/g. The question arises whether such values are absolute or whether they depend on the use of nitrogen as a probe. Further insight comes from analyzing results from adsorption experiments using differently sized molecules. It appears that the surface area S accessible to a molecular species is often not a constant but depends on the size of the molecules. More particularly, the larger the molecule, the smaller the accessible surface area.

About 15 years ago, Pfeifer, Avnir and Farin [41,53,54] made an important observation from the analysis of many adsorption data published in the literature: for a large number of porous media, including many catalysts, the measured surface area S depends on the effective diameter δ of the sorbate molecules according to a simple power law:

$$S \sim \delta^{-a} \quad (1)$$

More precisely, when the data are plotted as log$S$ versus logδ, a straight line can be fitted, with a slope a between 0 and 1. If $a = 0$, the surface area does not depend on the size of the probe. Frequently, however, $a > 0$, implying that 'specific area' is meaningless without specifying the resolution δ.

A few years earlier, fractal geometry was popularized by the bestseller of its founder Benoit Mandelbrot [39]. In 1967, using Richardson's observations, Mandelbrot had noted that a coastline's length depends on the resolution of the map, because irregularities repeat themselves at every scale and such that magnifications of details on the map are statistically indistinguishable from larger parts [55]. Maps at different resolutions are interchangeable. As a result, the length of a coastline is a power law of the scale δ:

$$L \sim \delta^{-a} \quad (2)$$

Length has no meaning, since it depends on the scale at which the coastline is observed; it even tends to infinity for $\delta \to 0$.

Mandelbrot discovered that coastlines are an example of a vast number of structures in Nature that have no characteristic scale. He called these structures *fractals*. Lightning, trees, mountains, clouds, lungs or kidneys: instead of becoming smoother upon magnification, the complexity, rugosity, fragmentation or branching is constantly self-repeating. Classical, Euclidean geometry is unable to describe these shapes in an easy way, but fractal geometry can by noting their inherent long-range order. Like for coastlines, details are often indistinguishable from the whole or from larger parts. It is this symmetry, *self-similarity* (in other cases, e.g., deposits or mountains, self-affinity), that allows us to solve physico-chemical problems on or around fractals, just like the translational symmetry of crystal lattices helps us to discover their properties.

Pfeifer and Avnir proposed that the pore walls of many 'amorphous' materials are, like coastlines, statistically self-similar fractals, yet on a molecular scale and in three dimensions [41,53,54]. With a remarkable insight, Adamson [43] noted already in 1960 the possible similarity between molecular roughness of catalyst surfaces and coastlines, and even noted, without using the term, the self-similarity of coastlines. However, this observation was left unnoticed until Avnir et al. rediscovered it [56], and it was the link with fractal geometry that gave the impetus to modeling surface roughness in a realistic way.

This is not the place to enter into the mathematical theory of fractals, which is discussed in many articles and books, such as [39,57]. Suffices to recall the meaning of *fractal dimension* D, which expresses the space filling capacity of a fractal. While Euclidean shapes have integer dimensions, e.g., 1 for a line, 2 for a surface and 3 for a volume, the dimension of a coastline can be any real number between 1 and 2. A catalyst surface can have any dimension between 2 and 3, both limits included. The dimension can never be larger than that of the space in which the set resides, 3 for catalyst surfaces, but it can be larger than the topological dimension, 2 for a surface. A nonfractal surface, like that of graphite, is two-dimensional. A self-similar fractal surface has an infinite area yet a zero volume: its dimension D lies between 2 and 3. Some fractal surfaces, such as those of certain gels, are so convoluted that they actually fill part of the available volume and their surface is three-dimensional ($D = 3$). The adsorbed volume, and not the area, is then independent of the molecular diameter δ. It is possible to define fractional s-dimensional measures that discontinuously drop from infinity to zero when s increases from slightly below to slightly above D. Informally, the number N of units of size δ needed to cover a fractal object decreases with δ as:

$$N \sim \delta^{-D} \quad (3)$$

Lengths are measured as $N\delta$, areas as $N\delta^2$, so that, in Eq. (2), $a = D - 1$ for coastlines, and in Eq. (1) for fractal surfaces, $a = D - 2$:

$$S \sim \delta^{2-D} \quad (4)$$

A real object can only be self-similar (or otherwise fractal) within a finite fractal *scaling range*, in between the so-called *inner and outer cutoffs*, $\delta_{\min}$ and $\delta_{\max}$.

In Fig. 1, the same segment of a cross-section of a fractal catalyst surface is shown twice, with a monolayer of adsorbed molecules. Small molecules, on the left, can adsorb within fjords or indentations to which large molecules, on the right, have no access. The self-similar cascade of fjords leads to a power law of the accessible area S as a function of δ.

Despite the measured power law behavior, additional experimental evidence is required to conclude

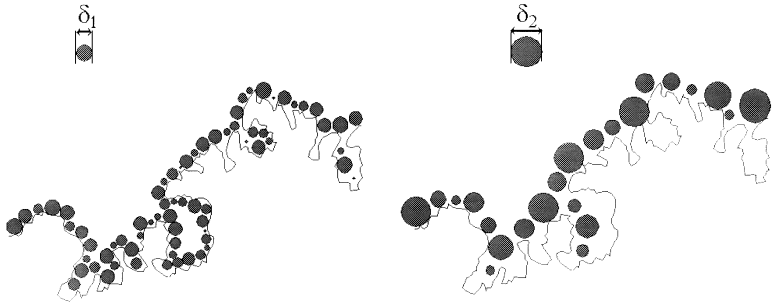

Fig. 1. Adsorption on a fractally rough surface. Small molecules, on the left, have access to a higher surface area than large molecules, on the right.

that a catalyst surface is fractal, because different molecular conformations, changes in adsorption energy and other factors can also contribute to an apparent change in surface area. Because the size of the sorbate molecules is not easily varied over a wide range, the method is insufficiently reliable to test power law behavior against other functional dependencies. It is usually impossible to determine the cutoffs: the cascade of fjords is limited by, at least, atomic dimensions on the one hand, and, e.g., by the size of the pores between the aggregates on the other hand.

To circumvent the disadvantages of the previous method, another technique using information from the complete adsorption isotherm of a single probe (typically nitrogen) was proposed by Neimark [58]. While this method is easy and appears effective, it is indirect and assumptions regarding the pore network topology need to be made. This pleads for another experimental method.

Small angle X-ray scattering (SAXS) [59,60], known in catalysis as a method to determine particle and sometimes pore size distributions, can be used to study the fractal mass and surface morphology of materials [61–63]. It has been used to investigate the morphology of rocks [3,62,64], coal particles, glasses [65,66], solid aerogels and aggregates in solution [61,67–69]. We found it to be equally effective to study the fractal surface morphology of industrial catalysts. Correlations in the geometry of the surface and the mass are derived from the evolution of the measured scattered intensity I as a function of the scattering angle θ. Results are shown as a function of the projected wave vector $q = (4\pi/\lambda)\sin(\theta/2)$; q is inversely proportional to the observation scale and plays the role of the inverse of the diameter of the molecules, δ, in the multiple probe adsorption method. Fig. 2 shows SAXS and WAXS (wide-angle scattering) results for a $PtRe/Al_2O_3$ catalyst used for the catalytic reforming of naphtha, an application to which we will come back in Section 5.2. By combining very small and small-angle scattering of intense X-ray synchrotron radiation with wide-angle X-ray scattering, the catalyst structure can be scanned on scales going from less than 1 Å up to 50 nm. From the straight slope in the log–log plot, the fractal dimension of the surface, here $D = 2.33$, is derived, and the leveling on both sides of the line yields the cutoffs: an inner cutoff of about 3 Å, and an outer cutoff of about 6–7 nm, the average pore diameter, consistent with nitrogen adsorption results. Note that heterogeneities in the chemical composition of the catalyst may also influence the scattering. In general, the intensity of the scattered radiation is proportional to the sum of the products, for each phase, of the volume fractions and the squared electron density deviations from the average. When the volume fraction of one of the phases is much larger than that of the other phases, such as is the case for the alumina in a catalytic reforming catalyst, most of the scattered intensity originates from that phase; in the example shown in Fig. 2 only 7% of the scattering can be attributed to the metal phase, so that the presence of the latter does not appreciably influence the results to the extent that it would change the general behavior or the slope of the log–log

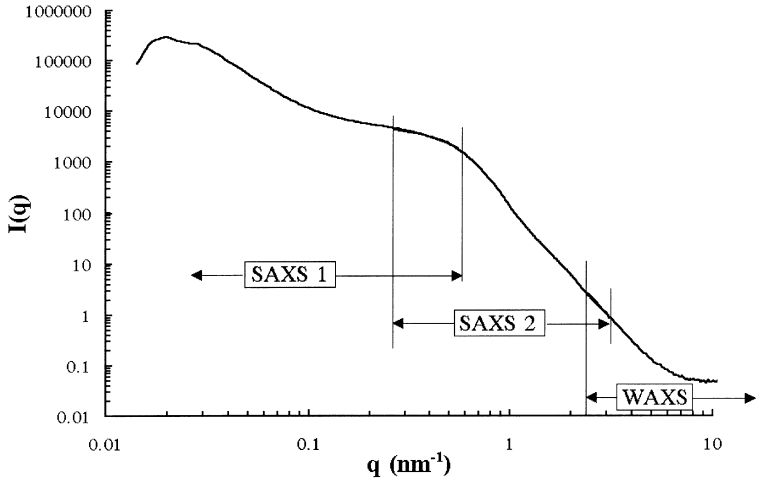

Fig. 2. Small-angle X-ray scattering (SAXS) and wide-angle X-ray scattering results for a $PtRe/Al_2O_3$ catalyst.

plot. However, effects from chemical heterogeneities need to be considered for heterogeneous catalysts with distinct strongly scattering phases, to ensure that the measurements are representative for the internal surface geometry; in a supported metal catalyst with a high fraction of metal, scattering from the metal-support and metal-pore interfaces will be stronger than from the (possibly fractal) support-pore interface.

Using the same method as for the reforming catalyst, a pure γ-alumina was also found to have a fractal surface, while, for a Y-type faujasite, the expected dimension 2 of a crystalline structure was recovered. This method does not have the previous disadvantages, at least if the chemical composition of the catalyst is sufficiently homogeneous. The results are satisfying, because they convincingly confirm the fractal surface morphology by determining the fractal dimension of the catalyst surface with high accuracy, as well as the cutoffs of the scaling regime.

Further evidence comes from the way the catalysts are prepared. The way a material is made reveals a lot about its structure and it is in general a good idea to test whether an investigated structure is generated through a recursive mechanism before performing a fractal scaling analysis, because recursion or iteration of growth, aggregation, fragmentation or branching is a natural pathway to fractals. Amorphous porous catalysts and catalyst supports are made by a series of steps that often starts with a sol–gel synthesis [44,70].

Growth and aggregation phenomena far from equilibrium are known to lead to fractal or fractal-like structures [40,71]. Fractal aggregates, such as the common DLA (diffusion-limited aggregate) [72] and CCAs (cluster-cluster aggregates) [73] grow through recursive polymerization and polycondensation reactions in a liquid or gas. During the sol–gel synthesis of aluminas, silicas, zirconias and other materials used in catalysis, such aggregates are formed quickly, far from equilibrium. Computer simulations [1,73,74] and experiments [1,67–69,75–77] provide plenty of evidence for their fractal nature. However, they are unstable and often rearrange already in solution to denser structures with a fractal surface. At higher concentrations of the sol, aggregates with a fractal surface can also be formed directly [78].

This gives a first clue as to why catalyst particles, consisting of aggregates of typically around 10 nm, can have a fractal surface. Nevertheless, it is not obvious that the formed fractal surface structure remains essentially conserved throughout the drying and, especially, the calcination steps following the preparation of the aggregates. Also impregnation to make multifunctional and composite catalysts or to deposit an active component on to a porous support can change the morphology. X-ray scattering, adsorption and other

experimental methods to test the final structure are therefore necessary. Together, they show the fractal surface morphology of many industrial catalysts, such as $PtRe/Al_2O_3$, in their final form.

3. Diffusion and reaction in fractal pores

3.1. The fractal pore model

Having demonstrated that a catalyst's internal surface is fractal, the geometry of the catalyst pores and its influence on diffusion and reaction can be studied. It has been recognized that the approximation of a porous catalyst particle by a homogeneous continuum is in general too coarse, because it neglects the interconnections between the pores, i.e., the *topology* of the pore network. Using such methods as percolation theory, the effective medium approximation, renormalization group theory and Monte-Carlo simulations, diffusion and reaction in pore networks has been studied in depth (for an excellent review, see [9]).

Nevertheless, as mentioned in the previous section, the *morphology*, i.e., the shape of the pores and of the pore walls, is usually neglected; pores are generally represented as simple bodies from Euclidean geometry, mostly cylinders, sometimes with spherical intersections. The roughness, previously difficult to describe mathematically [79], can now be accounted for in a realistic way, by replacing the straight, smooth, cylindrical pore channels by *fractal pores*, which can be tortuous and have a rough fractal surface.

Much of the research on diffusion and reaction in porous catalysts with a fractal internal surface has focused on the derivation of general, qualitative scaling laws expressing the power law dependency of certain properties on the observation scale [1]. A more quantitative study of the influence of the fractal surface morphology on diffusion and reaction was started by Coppens and Froment, and is reviewed in what follows [80–87]. Examples of models that assume the pore network or the catalyst itself – not only the surface – to be fractal were already cited in the introduction.

To separate the effects of the pore network topology from those of the pore shape, first an individual pore is studied in this section. Note also that despite the fundamental importance of network models, in many practical situations continuum models are sufficiently accurate for most catalysts [15,88]. Notable exceptions are networks close to a percolation threshold (e.g., due to deactivation), when some reactions are extremely rapid or when the molecules are of about the same size as a substantial subset of the pores.

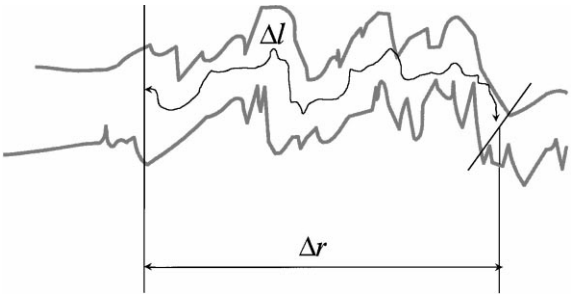

Fig. 3. Fractal pore model.

The basic equations of the fractal pore model are now shortly reviewed and an example, the production of vinyl acetate, is discussed. More details on this work can be read in [80–82].

3.2. Basic equations and general solutions

Consider, in Fig. 3, a section of a fractal pore. Such a pore has a fractal surface and is possibly tortuous. The pore segment has an axial length Δl. The cross-section, perpendicular to the axis, has an area Ω. A pore diameter may be defined as $d = 2\sqrt{\Omega/\pi}$.

Just like Euclidean geometry is used to derive a formula for the area of a cylinder, which is $\pi d \Delta l$, fractal geometry can be used to calculate the area ΔS accessible to molecules in this fractal channel segment. The latter depends on the diameter δ of the molecules: the area increases by a factor proportional to δ'^{2-D}. The effective diameter δ of the molecules has been normalized with respect to the outer cutoff of the fractal scaling regime, i.e., the size of the largest fjords, hence the prime ($'$) added to δ in this formula. From samples investigated by SAXS experiments, it follows that the outer cutoff δ_{max} is almost the same as the pore diameter d, although this need not be so in general.

In previous work [82], the symbol D^s_{ads} was used to stress that D is in fact the fractal dimension of the surface accessible to a molecule that adsorbs from

within the pore space. The simplified D is used in this paper.

For longer pores, the fractal surface roughness may induce a *pore tortuosity* leading to a shorter end-to-end distance (the distance in the r-direction in Fig. 3) than the distance along the pore axis (the l-direction), just like for linear polymers, which are also fractal. If the pore tortuosity is induced by the fractal surface roughness, the fractal dimension of the pore axis is $D-1$, so that $l \sim r^{D-1}$. In that case, the pore tortuosity is $(\delta^p_{\max}/\delta^p_{\min})^{D-2}$, in which $\delta^p_{\max}$ and $\delta^p_{\min} \approx d$ are the outer and the inner cutoff of the fractal scaling regime for the pore axis.

Many heterogeneously catalyzed processes are diffusion limited. It is well recognized that the pore geometry may influence the diffusivity. A variation in pore cross-section Ω along the axial coordinate, e.g., affects the *molecular diffusivity* [89–91]. If the pore is (fractally) tortuous, the gradient and flux in Fick's laws have to be considered with respect to the axis [81]. However, ordinary molecular diffusion of gas molecules is a result of intermolecular collisions and is only slightly influenced by the surface morphology.

This is altogether different for *Knudsen diffusion*, which is the dominant diffusion process when the frequency of collisions of the molecules with the surface is larger than or of the same order of magnitude as the frequency of intermolecular collisions. This situation frequently occurs in mesoporous catalysts under industrial operating conditions. In the Knudsen regime, gas molecules move in a straight line from one point on the accessible surface to another point. Since the cascade of fjords restricts molecular motion in fractal pores, Knudsen diffusivities are smaller than in smooth pores. For very long smooth cylindrical pores of diameter d, Knudsen derived the formula:

$$\mathcal{D}_{K0} = \frac{1}{3} d\overline{u} \tag{5}$$

in which $\overline{u} = \sqrt{8R_gT/\pi M}$ is the average molecular velocity [92]. He derived his formula using a momentum transfer approach, assuming the validity of the kinetic theory of free gases with a Maxwell velocity distribution. The formula was extensively verified through carefully carried out experiments in cylindrical tubes with a circular cross-section. However, he also proposed in his 1909 paper to extend the formula to tubes of arbitrary cross-section with area Ω and perimeter P:

$$\mathcal{D}_K = \frac{4}{3}\frac{\Omega}{P}\overline{u}. \tag{6}$$

This implies that the Knudsen diffusivity is inversely proportional to the accessible surface area, Eq. (4), so that for fractal pores:

$$\mathcal{D}_K = \mathcal{D}_{K0}(\delta')^{2-D} \tag{7}$$

in which $\mathcal{D}_{K0}$ is the Knudsen diffusivity in a smooth, cylindrical pore [81].

One year after Knudsen's pioneering publication, Smoluchowski [93] derived from purely geometrical arguments a more complex formula replacing Eq. (6). He showed that the mean-field argument that led to Eq. (6) can only hold for circles: in pores with differently shaped cross-sections, the accessibility along the perimeter is nonuniform, leading to deviations from Eq. (6). In particular, if for a fixed area Ω the perimeter P were infinite, Knudsen's formula would predict a zero diffusivity and flux, which is clearly incorrect. This situation occurs for fractal pores, for $\delta \to 0$, so that Eq. (7) can only be correct to a first approximation. A more accurate analytical formula will be derived in Section 4 and discussed in the light of recent Monte-Carlo simulations.

In the presence of a *surface process* such as reaction or adsorption, the fractal surface roughness could influence the effective reaction or adsorption rates if significant concentration gradients develop in the direction of the surface. Even within short cylindrical pores and ink-bottle pores, such gradients may develop [89,94,95]. The problem of molecular diffusion toward a fractal interface and uniform reaction or adsorption on that interface has been extensively studied in the literature, often employing the useful analogy with electrical conduction and a resistance at the surface [19,20,29,96–98]. However, these studies cannot be readily translated to mesoporous catalysts, because Knudsen diffusion and configurational effects usually prevail within the fractal fjords along the surface [80,87]. In general, except for very fast reactions or when the partial pressure of a reactant is very low, fractal roughness on molecular scales does not lead to pronounced additional gradients in the direction of the catalytic surface [80]. It should also be noted that the surface may be far from uniformly active on the scale

of the outer cutoff of the fractal scaling regime, δ_{max}, as in the important case of supported porous catalysts [80]. In this paper, diffusivities that were calculated in the absence of reactions will therefore be used in reaction studies, although it should be mentioned that on the scale of the smallest indentations along the surface, approaching molecular sizes, configurational effects similar to those found in zeolites may become important. This problem can only be seriously studied using truly microscopic approaches, such as molecular dynamics. The methods reviewed here are more 'mesoscopic' in nature, but reflect the major influence of fractal roughness on diffusion and reaction in a way suitable for engineering calculations.

Surface diffusion is clearly influenced by the surface morphology. Another paper in this volume [99] discusses this in more detail. Diffusion on a fractal surface is anomalous: if a molecule is adsorbed for a time t_s, the variance of the molecule's position scales as $\langle r^2 \rangle \sim (t_s)^{1/(D-1)}$, on the condition that the surface is chemically homogeneous and the distance in free flight is smaller than the outer cutoff of the fractal scaling regime, i.e., $\sqrt{\langle r^2 \rangle} < \delta_{max}$. However, chemical heterogeneities influence surface diffusion to an important degree. Since surface diffusion is usually activated, it is strongly temperature dependent. For many industrial processes catalyzed by a mesoporous catalyst, and using gases at higher temperatures and not too high pressures, surface diffusion is less important than Knudsen and molecular diffusion. Because of this, surface diffusion is not further discussed in this paper, yet the effect of fractal and other geometrical heterogeneities is an important problem when these conditions are not satisfied.

Experimental *reaction rates* are usually determined per unit catalyst mass, preferably under conditions where transport limitations are absent [100]. Therefore, the surface morphology does not influence the expressions to be used in a fractal model. However, in order to design a new catalyst with the same reaction rates per unit catalyst surface area or turnover frequency, but a higher fractal dimension D of the *active* phase, the reaction rates per unit catalyst mass should be corrected by the corresponding increase in surface area.

The previous observations enable the derivation of a *continuity equation* for diffusion and N_r reactions of a component j in a reacting mixture of M components:

$$-\frac{dN_j}{dl} = \left(\frac{S^l_{N_2}}{\Omega S^m_{N_2}}\right) \sum_{i=1}^{N_r} \alpha_{ij} r_i \tag{8}$$

where N_j is the molar flux of j, α_{ij} is the stoichiometric coefficient of the jth component in the ith reaction with reaction rate r_i, $S^l_{N_2}$ is the specific area per unit pore axial length accessible to a reference molecule, chosen to be nitrogen, and $S^m_{N_2}$ is the area accessible to nitrogen per unit catalyst mass [81]. Any other molecule could be chosen as a reference, since $S^l_{N_2}$ and $S^m_{N_2}$ scale in similar ways with the molecular diameter δ, but nitrogen adsorption is commonly used to measure a specific surface area, hence the choice. For a fractal pore:

$$S^l_{N_2} \approx 2\sqrt{\pi}\sqrt{\Omega}(\delta'_{N_2})^{2-D} = \pi d(\delta'_{N_2})^{2-D} \tag{9}$$

Eq. (8) is very similar to a classical continuity equation [100], yet there are three main differences: (1) the equation only holds along the pore axis (l), so that a pore tortuosity may have to be included to transform the results to real (r) space; (2) the right hand side now depends on the fractal dimension D of the surface; (3) the derivative on the left-hand side is actually an approximation for $\Delta N_j/\Delta l$, for $\Delta l = \delta_{max}$. The latter is usually allowed, under a broad range of conditions; for a single reaction, the Thiele modulus of the pore, to be defined later, should satisfy $\phi^p \ll l/\delta_{max}$, in which l is the pore length [81,82].

The fluxes and partial pressure gradients of the M components are related to each other through the Stefan–Maxwell equations for multicomponent diffusion:

$$\frac{dp_j}{dl} = -\frac{R_g T}{100}\left[\sum_{\substack{k=1\\k\neq j}}^{M}\left(\frac{p_k - p_j N_k/N_j}{p_t \mathcal{D}_{jk}}\right) + \frac{1}{\mathcal{D}_{Kj}(\delta_j)}\right] N_j \tag{10}$$

where the ideal gas law was used, fluxes are in kmol/m^2 s and partial pressures are in bar, $\mathcal{D}_{jk}$ are the morphology independent binary diffusivities and $\mathcal{D}_{Kj}$ the fractal morphology dependent Knudsen diffusivities [100–103].

The M continuity and M flux equations need to be solved simultaneously. Solutions for a first-order reaction are provided in [81]. The problem for a general single reaction is solved in [82], where a general-

ized Thiele modulus for a fractal pore is introduced, similar to the generalized modulus for catalyst pellets [100,104]:

$$\phi^p = l r_A(\boldsymbol{p}_0) \sqrt{\frac{R_g T S^l_{N_2}}{200\Omega \mathcal{D}_{\mathrm{Am}} S^m_{\mathrm{N_2}} \int_{p_{A0}}^{p_{Ae}} r_A(p_A)\,\mathrm{d}p_A}}. \quad (11)$$

Here, $\mathcal{D}_{\mathrm{Am}}$ is the effective diffusivity of the reference component A in the mixture and $\boldsymbol{p}_0 = (p_{A0}, \ldots, p_{M0})$. The modulus is defined by requiring that the effectiveness factor η^p be the inverse of ϕ^p for strong diffusional limitations ($\phi^p \to \infty$), similar to [104]. Under reaction limited conditions, $\eta^p = 1$. For intermediate conditions, $\eta^p \approx (\tanh \phi^p)/\phi^p$, where the approximation is exact for a first-order reaction in a dead-end pore. The Thiele modulus and the right hand side of Eq. (8) depend on the fractal roughness, mostly via $S^l_{\mathrm{N_2}}$ and, in the Knudsen diffusion limited regime, via the diffusivities, which also indirectly influence the integral of the reaction rate in the denominator. The latter dependence varies from component to component, so that it is generally impossible to construct an equivalent, smooth cylindrical pore that leads to the same partial pressure and flux profiles as those obtained for a fractal pore. The predicted conversions and selectivities will always differ.

3.3. Example: production of vinyl acetate

Fractal surface morphology effects, without reference to the pore network topology, are illustrated in the following example taken from [82]: the production of vinyl acetate (VAc) from ethylene, oxygen and acetic acid under industrial operating conditions ($p = 8$ bar, $T = 448$ K) in a 6 nm pore of the 1.0 wt.% Pd/Al_2O_3 catalyst which is used for this process. The surface of the mesopores is fractal with a fractal dimension of 2.79. The specific area measured by nitrogen is $S^m_{\mathrm{N_2}} = 192\ \mathrm{m^2/g}$ cat. Only the main reaction:

$$C_2H_4 + \tfrac{1}{2}O_2 + CH_3COOH \rightarrow C_2H_3OOCCH_3 + H_2O \quad (12)$$

is considered in this example; the CO_2 producing side reactions are neglected. Kinetics were taken from [105]. More details are provided in [82]. A comparison is made between the fractal pore and a smooth pore of the same length l and diameter, assuming the same catalyst area per unit mass measured by nitrogen, $S^m_{\mathrm{N_2}}$, and the same kinetics on a mass basis, since these are commonly determined.

The diffusivities in a fractal pore are smaller than in a smooth pore, because Knudsen diffusion plays an important role in the total molecular transport. In a smooth pore, the average diffusivity of oxygen is $\mathcal{D} = 8.73 \times 10^{-7}\ \mathrm{m^2/s}$; for vinyl acetate, it is $\mathcal{D} = 4.79 \times 10^{-7}\ \mathrm{m^2/s}$. In the fractal pore, the average diffusivity of oxygen, $\mathcal{D} = 1.21 \times 10^{-7}\ \mathrm{m^2/s}$, is larger than that of vinyl acetate, $\mathcal{D} = 0.98 \times 10^{-7}\ \mathrm{m^2/s}$, just like in a smooth pore, because lighter molecules move more easily than heavy ones. However, the surface roughness leads to a more pronounced decrease in diffusivity for oxygen (factor 7.2) than for vinyl acetate (factor 4.9), because oxygen molecules can enter narrower fjords than the larger vinyl acetate molecules. Therefore, they are more hindered in their movement than vinyl acetate molecules, so that the ratio of diffusivities is closer to 1 in a fractal pore (1.23) than in a smooth pore (1.82). In summary, Knudsen diffusivities of different molecules decrease as a result of the fractal morphology and they are closer to each other than if the surface were smooth.

Fig. 4 shows the ratio f of the production of vinyl acetate (VAc) in a fractal pore versus the one in a smooth pore, as a function of the length l of the compared pores. There are no diffusion limitations in short pores: molecules reach the active centers easily, so that f equals the ratio of the surface areas accessible to nitrogen per unit pore length ($S^l_{\mathrm{N_2}}$), in this case more than 7. In longer pores, the molecular supply is more difficult so that the reaction is diffusion limited. Because the diffusivities in a fractal pore are smaller than in a smooth pore, the reacted quantities become the same over large distances, and the effective reaction rate in a fractal pore can even fall below the rate in a smooth pore.

Comparing the partial pressure of VAc at the dead end of a fractal and a smooth pore of the same length shows that the pressure in the fractal pore is higher for short pores, but lower for long ones. In short pores less vinyl acetate is formed when the pore walls are smooth, and the products diffuse away more easily, so that the partial pressure of VAc at the end is low. In somewhat longer pores diffusion limitations take over, so that the partial pressure of VAc that cannot leave the pore increases in a fractal pore before it starts to

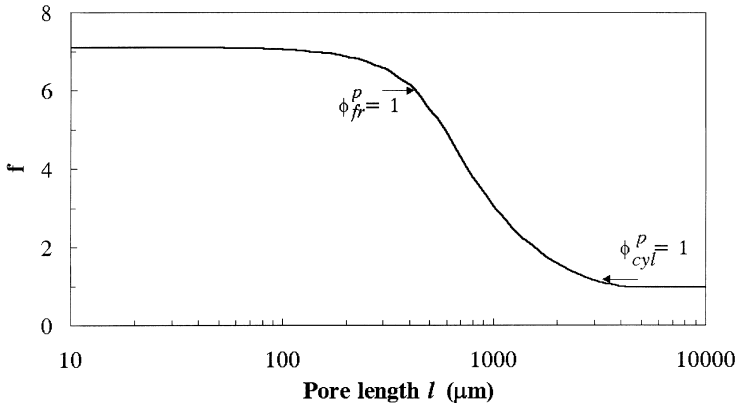

Fig. 4. Ratio f of the vinyl acetate production in a fractal versus a smooth pore, as a function of the pore length l (μm).

significantly increase in a smooth pore. For even longer pores the conversion of the reactants is complete, so that the partial pressure of the product VAc reaches a plateau value that is lower in a fractal pore, because the diffusivities of VAc and the lighter reactants are closer to each other than in a smooth pore. It is impossible to construct an equivalent cylindrical pore that would lead to the same conversion and partial pressures as a real fractal pore. Graphs and a comparison in terms of a generalized Thiele modulus are given in [82].

4. Effect of surface roughness on Knudsen diffusion

4.1. Fractal perturbation model

The next step is to investigate a complete catalyst particle, which contains a network of fractal pores. One approach is to connect the fractal pores discussed in the previous paragraph into a network that can in principle be reconstructed based on information from nitrogen adsorption, desorption and mercury porosimetry. This is far from trivial, however, and for many catalysts it is useful to model a porous catalyst particle with a fractal internal surface by superimposing fractal rugosity on top of the surface of a particle with a smooth internal surface. This is illustrated in Fig. 5. The smooth and the rough particles have the same pore network topology. A $PtRe/Al_2O_3$ reforming catalyst, e.g., consists of compressed alumina aggregates, so that the displayed packing of spheres plus a fractal roughness is a good model.

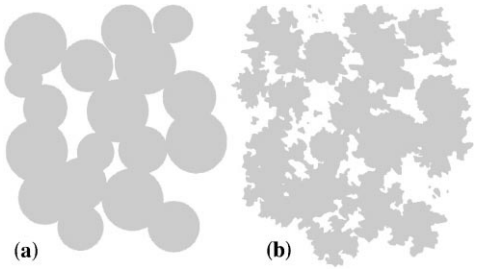

Fig. 5. Fractal perturbation model for porous catalysts. (a) non-perturbed packing of spheres; (b) aggregates formed by fractally perturbing (a).

Such a model allows to simplify the calculation of diffusivities by separating the effect of the fractal roughness, a new problem, from the calculation of diffusivities through a packing of overlapping spheres, a problem for which many solutions exist and which can be studied experimentally [106]. Fractal effects will now be studied in more detail for Knudsen diffusion, since it is expected from the nature of the phenomenon that roughness influences it.

4.2. Background on Knudsen diffusion in porous media

Knudsen diffusion in a porous medium remains a difficult, not well understood problem. As mentioned

earlier, Knudsen [92] made certain assumptions to derive Eqs. (5) and (6) that may not be valid. It is important to review those assumptions to study the complex problem of Knudsen diffusion in a porous material with a fractal internal surface.

Apart from the limitations of a mean-field approximation, only valid for isotropic problems, other problems persist. The velocity distribution is not Maxwellian due to the influence of the pore walls [93]. The axial velocity through a pore channel is not uniform, but depends on the distance from the wall; a similar distribution will be present in porous media [93,102]. Both problems are avoided using a geometrical approach, as favored by many authors.

Finite size effects influence the Knudsen diffusivity. In 1932, Clausing derived a formula for the diffusivity as a function of the channel length [107]. His approach is remarkably modern and transparent: the diffusivity is found from the transmission probability, which is calculated by solving a set of integral equations for the transmission and exit probabilities. The basis for his approach has often been used in much later years, not in the least because it is very useful in Monte-Carlo simulations, where the trajectories of molecules through a void space are followed to calculate the transmission probability [45–47,108]. Through a variational approach, Strieder derived a rigorous upper bound for the Knudsen and molecular diffusivity in a general porous medium, based on Clausing's integral equations [109–111]. Pore constrictions and the cross-sectional shape influence Knudsen diffusion [93,108,112–115].

The effect of surface irregularity has not been studied systematically, although it would already appear from the mentioned studies that it is important. Shallow roughness, on scales much smaller than the scale of the interstices or pores, was not found to play a major role [116,117], but fractal surface roughness in mesoporous materials may induce major perturbations on scales typically up to the size of the pores themselves. A description in terms of an average effective pore diameter gives useful first-order results: Eq. (5), e.g., was found to apply reasonably well to stacks of spheres [8,52]. However, the introduction of such an average implies a mean-field approach; the surface of spheres is concave, so that successive collisions are with different spheres. This is not the case with a convex, self-similar surface. A molecule may enter an indentation or fjord along the surface, collide with its walls, then move on to another point within the same fjord or move into a deeper fjord. It is possible for a molecule to make multiple wall collisions within a tree of fjords along the surface, before reappearing in the main pore space.

It is intuitively clear that the residence time of a molecule is on average higher in a tube or porous medium with a fractally rough surface than in the smooth, non-perturbed medium (in the language of the model presented above), since the trajectories of the molecules become more tortuous. For a fixed r.m.s. or end-to-end distance $\sqrt{\langle r^2 \rangle}$, the Knudsen diffusivity is inversely proportional to the average length l of the trajectories, due to Einstein's definition for the diffusivity. Therefore,

$$\frac{\mathcal{D}_K}{\mathcal{D}_{K0}} = \frac{l_0}{l}, \tag{13}$$

where the index 0 refers to the smooth, non-perturbed medium. Note that it is less obvious that the net flux through a tube is modified when the average 'effective' diameter, defined by $d = 2\sqrt{\Omega/\pi}$, is the same for fractally rough and smooth channels. Diffusivities measured using stationary and transient techniques can differ for porous media with dead-end and ink bottle pores, because there is no net flow through the latter, yet the average residence time and its variance are increased. A comparison of self and transport diffusivities in porous media will be the subject of a forthcoming paper [118].

It has been correctly assumed by Knudsen [92] that the reflections on the surface are diffuse. Molecules colliding with the surface leave it in a direction independent of the direction of incidence and following Lambert's cosine law, similar to diffuse light scattering. Surface roughness is frequently stated as a reason for this, but it has been shown by Clausing that this is not necessary to explain the cosine law, which is much more fundamental in nature and can be explained from the principles of microscopic reversibility and the second law of thermodynamics alone [112,119,120]. A condition is that the surface is isotropic and that the molecules adsorb for a sufficiently long time on the surface so that their translational energy is redistributed over all the degrees of freedom.

It is clear that a true detailed analysis of this problem should involve the interactions between gas molecules

and the surface atoms; this can be done by molecular dynamics [121]. It would be useful to apply molecular dynamics and grand canonical ensemble Monte-Carlo studies to fractally rough particles as well. Here the mesoscopic geometrical approach introduced by the author and which uses Eq. (13) is shortly reviewed [83,84].

4.3. Influence of fractal roughness on Knudsen diffusion

The Knudsen diffusivities in a porous medium with a fractal surface are smaller when the accessible surface area with which the molecules collide is larger: smaller molecules are more severely hindered by the fractal roughness than larger ones. But the inverse proportionality of the Knudsen diffusivities with respect to the geometrically accessible area, Eq. (7), only holds to a first approximation, since it is a mean-field result that assumes the surface to be *uniformly* accessible. This is clearly not the case for a fractal surface: some points on the rough surface are directly accessible, because they protrude into the pore space, while other points can only be reached after crossing several fjords and after multiple collisions. This nonuniform accessibility of the surface can also be accounted for.

In order to calculate the Knudsen diffusivity using Eq. (13), the first passage time t needed for a molecule to cross part of the catalyst pore space is compared with the shorter time t_0 needed to cross only the part that would be there if the surface were smooth. Only a single parameter additional to the fractal dimension of the surface is needed to calculate the ratio of the Knudsen diffusivities. This parameter p_0 is the probability for a molecule to leave a fjord, once it is in it. The problem can be analytically solved for a statistically self-similar surface by making use of the observation that a fjord tree bordering a given fjord with which a molecule collides has a similar structure to the larger tree including the fjord plus its sub-trees [83,84].

This leads to a Volterra integral equation of the second kind for the trajectory length or time spent in the fjord tree. After summing the distances spent by a molecule in the non-perturbed pore space and in the fractal fjord trees bordering it, use of Eq. (13) leads to the following practical, simple to use expression for the Knudsen diffusivity:

$$\frac{\mathcal{D}_K(\delta')}{\mathcal{D}_{K0}} = \frac{1}{1+\alpha\left[1-(\delta')^{\beta}\right]}, \tag{14}$$

in which:

$$\alpha = \frac{(2-D_C)(1+1/p_0)f}{1+(2-D_C)(1-1/p_0)} \quad \text{and} \quad \beta = 1+(2-D_C)\left(1-\frac{1}{p_0}\right), \tag{15}$$

and $f \approx 0.5$ for $\delta_{\max} = d$. The parameter D_C is explained in [83,84] and is found from:

$$D_C = \frac{2\log\gamma}{\log(1+\gamma)} \quad \text{with} \quad D = \frac{2\log\left((1/p_0)+\gamma\right)}{\log(1+\gamma)}. \tag{16}$$

Knudsen diffusion in packings of spheres or cylinders has been studied extensively, so that $\mathcal{D}_{K0}$ in the smooth medium is known, and the Knudsen diffusivity of the real medium can be calculated immediately.

The effect of the fractal surface roughness on the Knudsen diffusivity, $\mathcal{D}_K/\mathcal{D}_{K0}$, is shown in Fig. 6 for $\delta' = 0.1$ as a function of the fractal dimension of the surface, $D = D^s_{\text{ads}}$, and the return probability for a fjord, p_0, which needs to be smaller than a certain value that depends on the fractal dimension. The smaller the effective diameter of a molecule, δ', the lower its Knudsen diffusivity.

For not too extreme values of the return probability p_0, the most important parameter is the fractal dimension. If the fractal dimension is equal to 2 (e.g., for a smooth surface), then the ratio $\mathcal{D}_K/\mathcal{D}_{K0}$ is, by definition, 1. But for increasing fractal dimension, the Knudsen diffusivity decreases. There is a small maximum as a function of p_0. This is a consequence of the fact that an increase in p_0 increases both the probability to leave a fjord and the probability to enter it.

It is also interesting to look at the results for a particular surface with a certain fractal dimension, e.g., $D = 2.2$. Fig. 7 shows the normalized Knudsen diffusivity as a function of the normalized diameter δ' of a molecule; δ' lies between a maximum value, which is 1 after normalization, and a strictly positive minimum value, although the plot was extended down to $\delta' = 0$. The smaller a molecule is, the stronger the limitations imposed by the fractal roughness. The curves show results for different values of the return probability p_0. For extremely low p_0 the values are small,

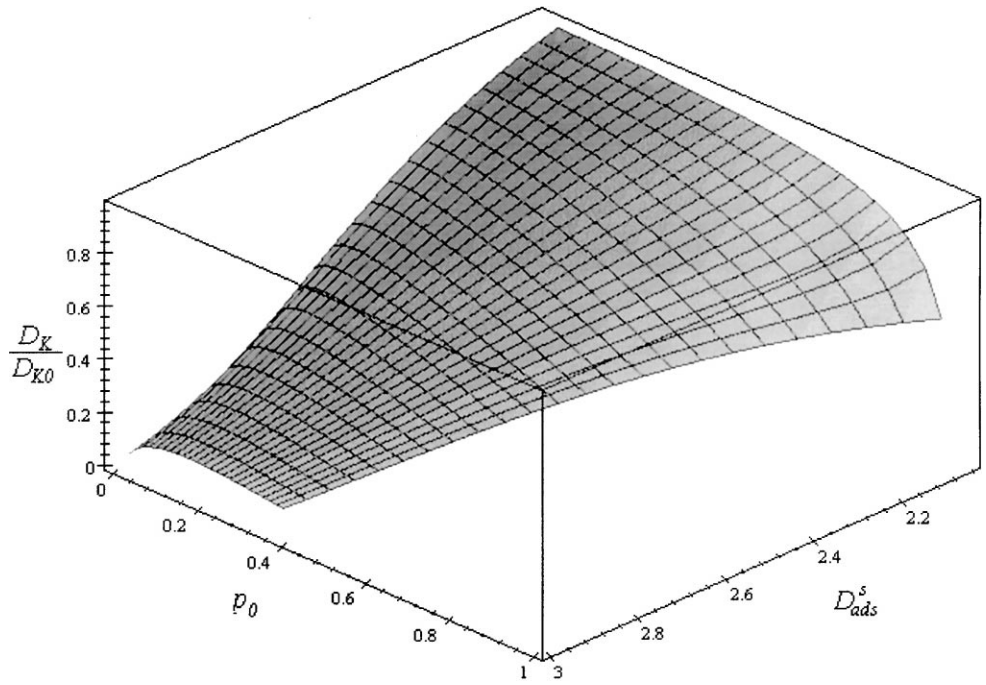

Fig. 6. Knudsen diffusivity of a molecule of a size 10 times smaller than the outer cutoff of the fractal scaling regime ($\delta' = 0.1$), normalized with respect to the diffusivity in a porous medium of the same topology, but with a smooth surface, $\mathcal{D}_K/\mathcal{D}_{K0}$.

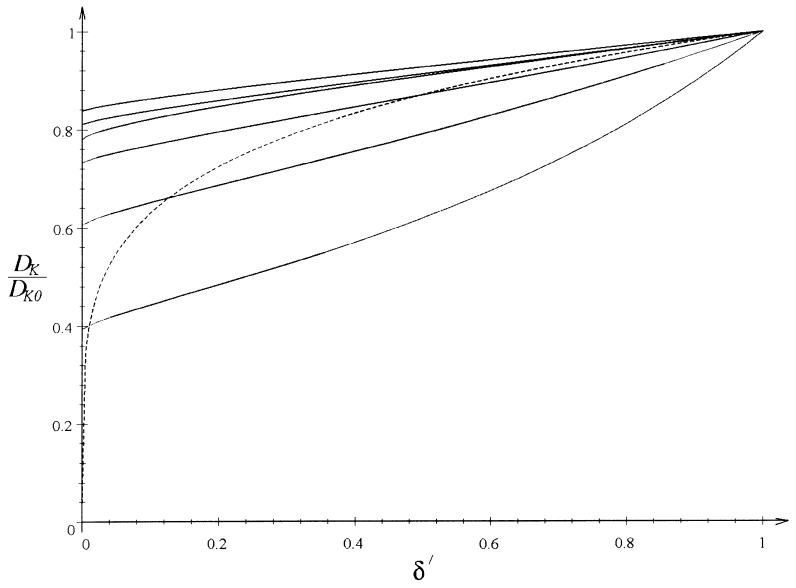

Fig. 7. Normalized Knudsen diffusivity, $\mathcal{D}_K/\mathcal{D}_{K0}$, as a function of the normalized molecular diameter, δ' for a porous medium whose surface has a fractal dimension $D = 2.2$. Full lines: from top to bottom, $p_0 = 0.1$, 0.2, 10^{-5}, 0.4, 0.6 and 0.791 ($p_{0,\max}$). Dotted line: mean-field result.

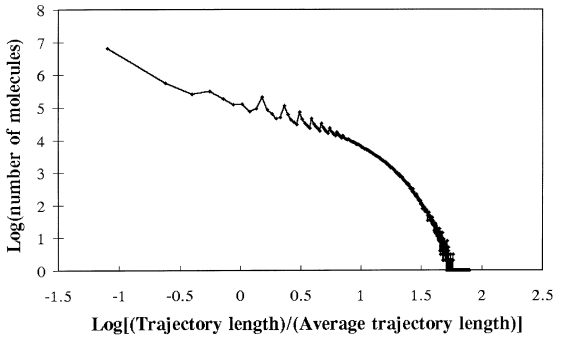

Fig. 8. Log–log histogram of the trajectory lengths for Knudsen diffusion in a Koch surface bordering a pore.

but for more realistic values the influence of p_0 is less pronounced. The dotted line shows results which do not account for the nonuniformity of the accessibility distribution, i.e. , the mean-field equation Eq. (7).

Sapoval performed two-dimensional simulations [117] that showed no appreciable influence of fractal surface roughness on the Knudsen diffusivity, but these were done in channels with an outer cutoff much smaller than the channel diameter. The above equations can be adapted to this situation, showing that the effects are indeed minor in that case.

Monte-Carlo simulations of diffusion in a pore with a deterministic fractal surface, namely a Koch surface, can reveal the origin for the decrease in diffusivity [87]. Fig. 8 shows a log–log histogram of the trajectory lengths of the molecules within a fractal fjord cascade. The length is normalized with respect to the average trajectory length. Within the fractal scaling regime for the surface, a power law is found. A large number of molecules does not enter into the cascade of fjords, as was also found by [117]. The largest fraction of molecules has a trajectory length which is smaller than the average length, but, apparently, the diffusion is dominated by the other molecules, smaller in number, which are trapped inside fjords and hence cover much longer distances.

If the same histogram is plotted on a semi-log scale, a long straight tail is found for long trajectories: the distribution is exponentially decreasing in this limit, because of the finite inner cutoff of the fractal scaling regime or because molecules cannot enter fjords smaller than themselves.

Both the analytical calculations and the Monte-Carlo simulations show that the fractal surface roughness increases the trajectory lengths and decreases the diffusivity, and that this decrease is a result of a relatively infrequent number of very long paths. Such so-called power-law or Lévy statistics are typical for processes on and around fractals.

5. Reactor simulations and catalyst design

5.1. Basic equations

As discussed in Section 3.1, the equations for diffusion and reaction in a catalyst particle with a fractal internal surface are not different from those for classical particles, if the outer cutoff of the scaling regime is much smaller than the size of the particles, which is usually the case (δ_{max} is related to the aggregate or pore sizes). In the present model, all the information about the influence of the fractal morphology is condensed in the modified expressions for the Knudsen diffusivity and in the reaction rate equations. Other parameters remain essentially constant. If the surface morphology of the porous catalyst is changed and the intrinsic kinetics r_i (in the absence of diffusion) of a reaction i catalyzed by sites on that surface are known on a mass basis, r_i should be corrected for changes in accessible surface area. An example is an isomerization reaction on the alumina surface of a catalytic reforming catalyst. If, on the other hand, reaction i occurs on a nonfractal surface, and a change in fractal dimension of the fractal support is investigated at constant loading of the active phase for i, the reaction rate need not be changed. An example is a hydrogenolysis reaction on the Pt surface of a catalytic reforming catalyst – the platinum nanoparticles do not have a fractal surface.

For the example discussed below, a continuum model can be used at scales superior to the size of the mesopores. There may be additional heterogeneities at larger scales, but these pertain to the pore network and are contained within the value of the network tortuosity [122,123]. The derivation of the general equations and their solution method are discussed in [85] (see also [89]). Only the principle equations and methodology are given here.

The reactor equations are those of basic chemical reactor engineering: for a fixed bed reactor they include M continuity equations for each of the M components, an energy equation and a pressure drop equation [100]. At each location in the reactor where the conditions change, the effective reaction rates have to be recalculated. They may differ from the intrinsic reaction rates due to transport limitations. Intraparticle diffusion limitations are accounted for by solving the set of M continuity equations for multi-component diffusion and reaction in a catalyst pellet:

$$-(\nabla\mathcal{K})(\mathcal{K}^{-1}\nabla\boldsymbol{p}) + \nabla^2\boldsymbol{p} + 10^{-2}\rho_s R_g T\mathcal{K}\boldsymbol{R} = 0 \tag{17}$$

in which $(\nabla\mathcal{K})(\mathcal{K}^{-1}\nabla\boldsymbol{p})$ is short for $\sum_{i=1}^{3}(\partial\mathcal{K}/\partial x_i)\,\mathcal{K}^{-1}(\partial\boldsymbol{p}/\partial\boldsymbol{x}_i)$ in an orthonormal coordinate system (x_1, x_2, x_3). The non-diagonal elements of the Stefan–Maxwell matrix $\mathcal{K}$ are given by:

$$\mathcal{K}_{jk} = -\frac{p_j}{p_t\mathcal{D}_{e,jk}} = -\frac{p_j}{\mathcal{D}'_{e,jk}}, \quad k \neq j \tag{18}$$

and the diagonal elements are:

$$\mathcal{K}_{jj} = \frac{1}{\mathcal{D}_{e,Kj}} + \sum_{\substack{k=1\\k\neq j}}^{M}\frac{p_k}{p_t\mathcal{D}_{e,jk}} = \frac{1}{\mathcal{D}_{e,Kj}} + \sum_{\substack{k=1\\k\neq j}}^{M}\frac{p_k}{\mathcal{D}'_{e,jk}} \tag{19}$$

in which $\mathcal{D}_{e,Kj}$ are the effective Knudsen diffusivities and:

$$\mathcal{D}'_{e,jk} = p_t\mathcal{D}_{e,jk} \tag{20}$$

are the products of the total pressure and the binary molecular diffusivities. For not too high pressures, these products are pressure independent. The derivation of these general equations is discussed in [85]. The effective diffusivities are calculated using the perturbation model discussed in the previous section. The non-fractal contributions follow from an appropriate smooth model for the catalyst, e.g., a packing of overlapping or non-overlapping spheres.

Solving Eq. (17) for isothermal catalyst pellets with the bulk temperature, partial and total pressures as boundary conditions yields the partial pressure profiles within the pellets and the effective reaction rates, which can then be substituted into the reactor equations at that point. For a fixed bed reactor modeled using a one-dimensional heterogeneous plug flow model, for example, the set of $M + 2$ reactor equations is solved by moving step by step along the axis, typically using a method that can handle both stiff and non-stiff differential equations. At each step, the effective reaction rates are evaluated by integrating the set of M catalyst particle equations, typically using orthogonal collocation [85,124–127].

5.2. Example: catalytic reforming of naphtha

Using the previous method, this example illustrates the results for an important refinery process that utilizes a porous catalyst with a fractal internal surface: the catalytic reforming of naphtha, used to increase the octane number of gasoline and to produce benzene, toluene and xylenes.

The simulated industrial unit consists of four adiabatic reactors with a fixed bed of catalyst. Naphtha is fed into the first reactor, together with a recycle of flashed off light products, especially hydrogen, to limit coking. Most reactions are endothermal, so that the reaction mixture is heated before entering each reactor. The reformed naphtha is sent to a stabilisation column. Details on the unit and the operating conditions are provided in [85,86].

The goal of the process is to increase the aromatics content and to increase the fraction of branched iso-paraffins, starting from naphthenes and *n*-paraffins, which increases the octane number. A lot of hydrogen is formed. The reaction network of this process and its kinetics are very complex and were derived by Froment and co-workers [128–133]. It consists of 86 reactions between 28 hydrocarbon lumps and hydrogen gas. The components within each lump or group are in mutual equilibrium. The nonlinear reaction rate equations with their parameters were determined for each reaction. The hydrocarbons have 1 to 11 carbon atoms. Normal and single branched iso-paraffins can isomerize with formation of more strongly branched iso-paraffins. Paraffins can dehydrocyclize to form naphthenes, which can isomerize by ring expansion. Naphthenes are further converted into aromatics. Finally, undesired hydrocracking and hydrogenolysis convert part of the products into light paraffins.

A mesoporous $PtRe/Al_2O_3$ catalyst is used. Hydrogenations and dehydrogenations are catalyzed by

active centers on the metal crystallites, which are not fractal, but the active centers for isomerization reactions are acid centers on the alumina surface, which is fractal with a fractal dimension of about 2.3, as known from the previously discussed SAXS experiments (Fig. 2 in Section 2). The catalyst is described as a packing of overlapping fractally rough spheres; in between those spheres lies the pore space.

Several of these reactions are strongly diffusion limited and the equations and method discussed earlier in this section were programmed to perform catalyst particle and reactor simulations, so as to obtain the partial pressure profiles within the catalyst particles at any height in the reactors, as well as the temperature, total and partial pressure profiles of all the components throughout the unit.

It was first shown in [85] that the incorrect assumption of a smooth alumina surface leads to different results from those obtained if the surface is correctly taken to be fractal. In [86], simulations were performed at the same typical industrial operating conditions, but with an alumina with a fractal dimension D changing between 2 and 3. In other words, the question was raised what the influence from purely geometrical factors would be if the fractal surface morphology of the alumina were changed in a new catalyst design, which can be done by modifying the preparation conditions during the sol–gel synthesis.

The simulations showed that the partial pressure profiles were very different both within the catalyst pellets and within the reactors. Figures and a discussion of the results can be found in [86]. Here, it suffices to show and discuss a few summarizing results at the outlet of the industrial unit. In Fig. 9, the yields of two important product groups – aromatics and iso-paraffins – are plotted as a function of the fractal dimension of the alumina surface, $D = D^s_{\mathrm{ads}}$. Lumping components into main product groups is done only after detailed simulations considering all 29 components.

The aromatics yield increases with D, since it is a main product of the process and the available surface area for several reactions that finally lead to aromatics increases with D. At the same time, the iso-paraffin yield decreases: at higher D more iso-paraffins are formed from normal paraffins, but this mainly occurs in the first one of the four reactors. After that, much of the iso-paraffins is further converted into naphthenes and finally to aromatics, leading to a decrease of the

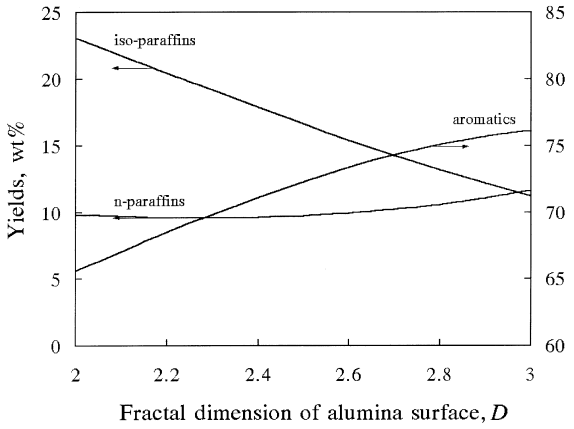

Fig. 9. Aromatics, iso-and normal-paraffin yields at the outlet of an industrial unit for the catalytic reforming of naphtha, as a function of the fractal dimension of the $PtRe/Al_2O_3$ catalyst.

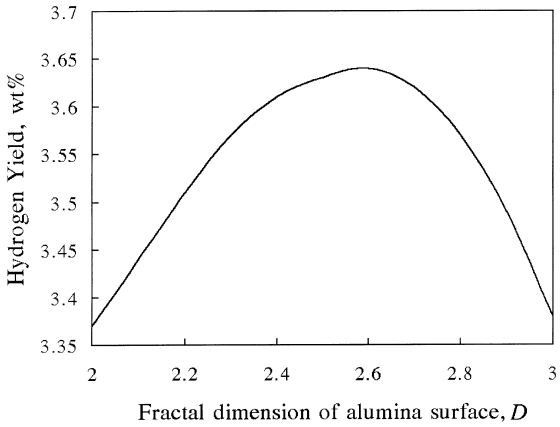

Fig. 10. Hydrogen yield at the outlet of an industrial unit for the catalytic reforming of naphtha, as a function of the fractal dimension of the $PtRe/Al_2O_3$ catalyst.

yield with D, because of the increased rate of the naphthene producing reactions.

Dehydrocyclization reactions and reactions that form aromatics from naphthenes produce hydrogen. This should lead to an increase of the hydrogen yield with fractal dimension D. However, as seen in Fig. 10, the hydrogen yield goes through a maximum. This is because several reactions are strongly diffusion limited. Hydrogen being the smallest molecule, it is relatively more restricted in its movement than the larger hydrocarbon molecules at higher fractal

dimensions of the surface. The molecules are trapped in small fjords, leading to enhanced hydrogenolysis and hydrocracking side reactions that convert the precious reaction products to light gases. Beyond the maximum around $D = 2.6$, hydrocracking becomes too significant. As a result, the increase in aromatics in Fig. 9 is smallest at high fractal dimensions, because part of the aromatics is consumed by the undesired hydrocracking and hydrogenolysis reactions, which become more and more important when the surface is rougher. The yield of iso-paraffins, another desired product, drops in an almost linear way with increasing fractal dimension, from 23% on a smooth surface to about half this value on an extremely rough surface.

There is not only a significant effect of the fractal morphology of the catalyst surface on the product distributions, even at the exit of an industrial unit, but a change in the fractal morphology by changing the catalyst preparation conditions has a significant impact on the process: pushing the fractal dimension form the present 2.3 up to 2.6, would produce a gasoline with more aromatics and a higher octane number, without too many side reactions. If the aromatics content has to remain low for environmental reasons then 2.3, with a high iso-paraffins content, is a good compromise.

One of the most important results is undoubtedly the effect of the fractal dimension of the alumina surface on the octane number of the produced gasoline. Fig. 11 shows a continuous increase of this index with increasing fractal dimension, because of the larger aromatics yield. The increase is less important for larger fractal dimensions, because of enhanced cracking, leading to undesired light products, so that there is an optimum.

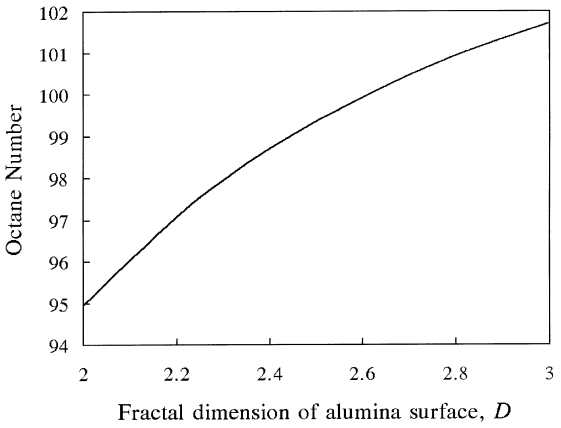

Fig. 11. Octane number of the produced gasoline, as a function of the fractal dimension of the $PtRe/Al_2O_3$ catalyst.

Hegedus and Pereira stress the immense opportunities offered by a rational catalyst design [134]. The present example illustrates that purely geometrical changes, even on a microscopic scale, can indeed have drastic effects on the global process.

6. Conclusions

Adsorption experiments suggested that the internal surface of many porous materials is fractal. SAXS experiments, presented in this paper, confirm this convincingly for several industrial 'amorphous' catalysts and catalyst supports. By combining SAXS and WAXS, it is possible to bracket the fractal scaling regime and to accurately estimate the fractal dimension of the catalyst surface. The fractal surface geometry is a result of the way in which these catalysts are prepared.

Using fractal geometry, the effects of roughness on diffusivities and reaction rates, and therefore also on conversions and product distributions, can be calculated. Reactions of the molecules on active sites on the surface that catalyze these reactions are often diffusion limited. Formulas that account for the fractal roughness of the pore walls are reviewed first for individual pore channels, then for complete catalyst particles.

Fractal effects prove to be significant and are felt not only on the scale of an individual catalyst pore or a single catalyst particle, but down to the outlet of an industrial reactor. This is illustrated for the production of vinyl acetate and the catalytic reforming of naphtha. Fractal geometry can therefore be a useful tool to optimize heterogeneously catalyzed processes.

Acknowledgements

Dr. H. Kuypers and Dr. R. Haswell from Shell Research and Technology Center Amsterdam are gratefully acknowledged for the SAXS and WAXS experiments. Useful initial experiments were made by Dr. A. Jonas from Université Catholique de Louvain, Belgium. Discussions with Professors G.R. Gavalas, E. Iglesia, B. Sapoval and S.V. Sotirchos helped to clar-

ify the conditions under which Knudsen diffusion depends on surface roughness. This project was partially carried out with funding through an 'aspirant'ship and a postdoctoral fellowship from the Fund for Scientific Research – Flanders, Belgium (F.W.O.).

References

[1] D. Avnir, The Fractal Approach to Heterogeneous Chemistry, Wiley, New York, 1989.
[2] P.M. Adler, Porous Media: Geometry and Transports, Butterworth–Heinemann Series in Chemical Engineering, 1992.
[3] M. Sahimi, Rev. Mod. Phys. 65 (1993) 1393.
[4] M. Sahimi, Applications of Percolation Theory, Taylor & Francis, London, 1994.
[5] F.J. Keil, Chem. Engng. Sci. 51 (1996) 1543.
[6] Y. Gefen, A. Aharony, S. Alexander, Phys. Rev. Lett. 50 (1983) 77.
[7] S. Reyes, K.F. Jensen, Chem. Engng. Sci. 40 (1985) 1723.
[8] S. Reyes, E. Iglesia, K.F. Jensen, Solid State Ionics 32/33 (1989) 833.
[9] M. Sahimi, G.R. Gavalas, T.T. Tsotsis, Chem. Engng. Sci. 45 (1990) 1443.
[10] F.A.L. Dullien, Porous Media – Fluid Transport and Pore Structure, 2nd ed., Academic Press, New York, 1992.
[11] D. Stauffer, A. Aharony, Introduction to Percolation Theory, 2nd ed., Taylor & Francis, London, 1992.
[12] C. McGreavy, M.A. Siddiqui, Chem. Engng. Sci. 35 (1980) 3.
[13] V.N. Burganos, S.V. Sotirchos, A.I.Ch.E. J. 33 (1987) 1678.
[14] P.N. Sharratt, R. Mann, Chem. Engng. Sci. 42 (1987) 1565.
[15] L. Zhang, N.A. Seaton, A.I.Ch.E. J. 38 (1992) 1816.
[16] M.P. Hollewand, L.F. Gladden, Chem. Engng. Sci. 47 (1992) 2757.
[17] J. Villermaux, D. Schweich, J.-R. Authelin, C. R. Acad. Sc. Paris Série II 304 (1987) 399.
[18] M. Sheintuch, S. Brandon, Chem. Engng. Sci. 44 (1989) 69.
[19] R. Gutfraind, M. Sheintuch, Chem. Engng. Sci. 47 (1992) 2787.
[20] R. Gutfraind, M. Sheintuch, Chem. Engng. Sci. 47 (1992) 4425.
[21] P. Mougin, M. Pons, J. Villermaux, Chem. Engng. Sci. 51 (1996) 2293.
[22] C. Gavrilov, M. Sheintuch, A.I.Ch.E. J. 43 (1997) 1691.
[23] L.W. Anacker, R. Kopelman, J. Chem. Phys. 81 (1984) 6402.
[24] R. Kopelman, in: D. Avnir (Ed.), The Fractal Approach to Heterogeneous Chemistry, Wiley, New York, 1989, p. 295.
[25] W.-S. Sheu, K. Lindenberg, R. Kopelman, Phys. Rev. A 42 (1990) 2279.
[26] S. Havlin, D. Ben-Avraham, Adv. Phys. 36 (1987) 695.
[27] M. Giona, Chem. Engng. Sci. 47 (1992) 1503.
[28] M. Giona, W.A. Schwalm, A. Adrover, M.K. Schwalm, Chem. Engng. Sci. 51 (1996) 2273.
[29] P. Meakin, Chem. Phys. Lett. 123 (1986) 428.
[30] S.S. Tambe, P. Badola, B.D. Kulkarni, Chem. Phys. Lett. 173 (1990) 67.
[31] T. Elias-Kohav, M. Sheintuch, D. Avnir, Chem. Engng. Sci. 46 (1991) 2787.
[32] D.E. Rosner, P. Tandon, A.I.Ch.E. J. 40 (1994) 1167.
[33] C.-K. Lee, S.-L. Lee, Sur. Sci. 325 (1995) 294.
[34] C.-K. Lee, S.-L. Lee, Sur. Sci. 339 (1995) 171.
[35] S.P. Rigby, L.F. Gladden, J. Catal. 180 (1998) 44.
[36] M.-O. Coppens, G.F. Froment, Fractals 5 (1997) 493.
[37] M.-O. Coppens, G.F. Froment, in: M. Giona, G. Biardi (Eds.), Fractals and Chaos in Chemical Engineering, World Scientific, Singapore, 1997, p. 15.
[38] M.-O. Coppens, A.I.Ch.E. Symp. Ser. Annual Meeting, Paper 101d, 1998.
[39] B.B. Mandelbrot, The Fractal Geometry of Nature, Updated and Augmented, Freeman, New York, 1983.
[40] T. Vicsek, Fractal Growth Phenomena, 2nd ed., World Scientific, Singapore, 1992.
[41] D. Avnir, D. Farin, P. Pfeifer, Nature 308 (1984) 261.
[42] M. Ben Ohoud, F. Obrecht, L. Gatineau, P. Levitz, H. Va Damme, J. Coll. Int. Sci. 124 (1988) 156.
[43] A.W. Adamson, Physical Chemistry of Surfaces, Wiley, New York, 1960.
[44] B.G. Linsen, Physical and Chemical Aspects of Adsorbents and Catalysts, Academic Press, New York, 1970.
[45] J.W. Evans, M.H. Abbasi, A. Sarin, J. Chem. Phys. 72 (1980) 2967.
[46] M.H. Abbasi, J.W. Evans, I.S. Abramson, A.I.Ch.E. J. 29 (1983) 617.
[47] K.A. Akanni, J.W. Evans, I.S. Abramson, Chem. Engng. Sci. 42 (1987) 1945.
[48] Y. Nakano, J.W. Evans, J. Chem. Phys. 78 (1983) 2568.
[49] J.A. Quiblier, J. Coll. Int. Sci. 98 (1984) 84.
[50] V.N. Burganos, S.V. Sotirchos, Chem. Engng. Sci. 44 (1989) 2451.
[51] V.N. Burganos, S.V. Sotirchos, Chem. Engng. Sci. 44 (1989) 2629.
[52] S.C. Reyes, E. Iglesia, J. Catal. 129 (1991) 457.
[53] D. Avnir, D. Farin, P. Pfeifer, J. Chem. Phys. 79 (1983) 3566.
[54] P. Pfeifer, D. Avnir, J. Chem. Phys. 79 (1983) 3558.
[55] B.B. Mandelbrot, Science 155 (1967) 636.
[56] D. Avnir, D. Farin, P. Pfeifer, New J. Chem. 16 (1992) 439.
[57] J. Feder, Fractals, Plenum Press, New York, 1988.
[58] A. Neimark, Physica A 191 (1992) 258.
[59] O. Glatter, O. Kratky, Small Angle X-Ray Scattering, Academic Press, New York, 1982.
[60] A. Guinier, G. Fournet, C.L. Walker Jr., K.L. Yudowitch, Small-Angle Scattering of X-Rays, Wiley, New York, 1955.
[61] H.D. Bale, P.W. Schmidt, Phys. Rev. Lett. 53 (1984) 596.
[62] P.W. Schmidt, in: D. Avnir (Ed.), The Fractal Approach to Heterogeneous Chemistry, Wiley, New York, 1989, p. 67.
[63] P.W. Schmidt, J. Appl. Cryst. 24 (1991) 414.
[64] P.-Z. Wong, A.J. Bray, Phys. Rev. B 37 (1988) 7751.
[65] D. Rojanski, D. Huppert, H.D. Bale, X. Dacai, P.W. Schmidt, D. Farin, A. Seri-Levy, D. Avnir, Phys. Rev. Lett. 56 (1986) 2505.
[66] A. Höhr, H.-B. Neumann, P.W. Schmidt, P. Pfeifer, D. Avnir, Phys. Rev. B 38 (1988) 1462.
[67] D.W. Schaefer, K.D. Keefer, Phys. Rev. Lett. 53 (1984) 1383.

[68] D.W. Schaefer, J.E. Martin, P. Wiltzius, D.S. Cannell, Phys. Rev. Lett. 52 (1984) 2371.
[69] K.D. Keefer, D.W. Schaefer, Phys. Rev. Lett. 56 (1986) 2376.
[70] J.F. Le Page, Applied Heterogeneous Catalysis: Design, Manufacture, Use of Solid Catalysts, Technip, Paris, 1987.
[71] D.A. Kessler, J. Koplik, H. Levine, Adv. Phys. 37 (1988) 255.
[72] T.A. Witten Jr., L.M. Sander, Phys. Rev. Lett. 47 (1981) 1400.
[73] M. Kolb, R. Botet, R. Jullien, Phys. Rev. Lett. 51 (1983) 1123.
[74] P. Meakin, Phys. Rev. Lett. 51 (1983) 1119.
[75] D.A. Weitz, M. Oliveria, Phys. Rev. Lett. 52 (1984) 1433.
[76] S.S. Kumru, H.D. Bale, J. Appl. Cryst. 27 (1994) 682.
[77] Y.W. Zeng, P. Riello, A. Benedetti, G. Fagherazzi, J. Non-Cryst. Sol. 185 (1995) 78.
[78] M. Kolb, H.J. Herrmann, Phys. Rev. Lett. 59 (1987) 454.
[79] L.M. Pismen, Chem. Engng. Sci. 29 (1974) 1227.
[80] M.-O. Coppens, G.F. Froment, Chem. Engng. Sci. 50 (1995) 1013.
[81] M.-O. Coppens, G.F. Froment, Chem. Engng. Sci. 50 (1995) 1027.
[82] M.-O. Coppens, G.F. Froment, Chem. Engng. Sci. 49 (1994) 4897.
[83] M.-O. Coppens, G.F. Froment, Fractals 3 (1995) 807.
[84] C.J.G. Evertsz, H.-O. Peitgen, R.F. Voss (Eds.), Fractal Geometry and Analysis, The Mandelbrot Festschrift, World Scientific, Singapore, 1996, p. 403.
[85] M.-O. Coppens, G.F. Froment, Chem. Engng. Sci. 51 (1996) 2283.
[86] M.-O. Coppens, G.F. Froment, Chem. Engng. J. 64 (1996) 69.
[87] M.-O. Coppens, in: J. Lévy-Véhel, E. Lutton, C. Tricot (Eds.), Fractals in Engineering, Springer, Berlin, 1997, p. 336.
[88] L. Zhang, N.A. Seaton, Chem. Engng. Sci. 49 (1994) 41.
[89] R. Aris, The Mathematical Theory of Diffusion and Reaction in Permeable Catalysts, vol. 1, Clarendon Press, Oxford, 1975.
[90] E.E. Petersen, A.I.Ch.E. J. 4 (1958) 343.
[91] A.S. Michaels, A.I.Ch.E. J. 5 (1959) 270.
[92] M. Knudsen, Ann. Phys. 4 F 28 (1909) 75.
[93] M. von Smoluchowski, Ann. Phys. 4 F 33 (1910) 1559.
[94] K.B. Bischoff, Ind. Engng. Chem. Fund. 5 (1966) 135.
[95] C. Chu, K. Chon, J. Catal. 17 (1970) 71.
[96] T. Pajkossy, L. Niykos, Electrochim. Acta 34 (1989) 171.
[97] B. Sapoval, in: A. Bunde, S. Havlin (Eds.), Fractals in Disordered Systems, Springer, Berlin, 1991.
[98] A. Seri-Levy, D. Avnir, Surf. Sci. 248 (1991) 258.
[99] S.P. Rigby, this volume.
[100] G.F. Froment, K.B. Bischoff, Chemical Reactor Analysis and Design, 2nd ed., Wiley, New York, 1990.
[101] R.B. Bird, W.E. Stewart, E.B. Lightfoot, Transport Phenomena, Wiley, New York, 1960.
[102] R. Jackson, Transport in Porous Catalysts, Elsevier, Amsterdam, 1977.
[103] R. Krishna, Chem. Engng. Sci. 48 (1993) 845.
[104] K.B. Bischoff, A.I.Ch.E. J. 11 (1965) 351.
[105] S. Nakamura, T. Yasui, J. Catal. 17 (1970) 366.
[106] D.G. Huizenga, D.M. Smith, A.I.Ch.E. 32 (1986) 1.
[107] P. Clausing, Ann. Phys. 5 F 12 (1932) 961.
[108] D.H. Davis, J. Appl. Phys. 31 (1960) 1169.
[109] W.C. Strieder, S. Prager, Phys. Fluids 11 (1968) 2544.
[110] W. Strieder, J. Chem. Phys. 52 (1970) 5204.
[111] W. Strieder, J. Chem. Phys. 54 (1971) 4050.
[112] P. Clausing, Ann. Phys. 5 F 7 (1930) 569.
[113] B.D. Eldridge, L.F. Brown, A.I.Ch.E. J. 22 (1976) 942.
[114] Y. Nakano, S. Iwamoto, I. Yoshinaga, J.W. Evans, Chem. Engng. Sci. 42 (1987) 1577.
[115] V.N. Burganos, A.C. Payatakes, Chem. Engng. Sci. 47 (1992) 1383.
[116] T.E. Holt, D.M. Smith, Chem. Engng. Sci. 44 (1989) 779.
[117] S.B. Santra, B. Sapoval, Phys. Rev. E 57 (1998) 6888.
[118] M.-O. Coppens, in preparation.
[119] P. Clausing, Ann. Phys. 5 F 4 (1930) 533.
[120] P. Clausing, Ann. Phys. 5 F 4 (1930) 567.
[121] J.M.D. MacElroy, K. Raghavan, J. Chem. Phys. 93 (1990) 2068.
[122] S.P. Rigby, L.F. Gladden, Chem. Engng. Sci. 51 (1996) 2263.
[123] S.P. Rigby, L.F. Gladden, J. Catal. 173 (1998) 484.
[124] J. Villadsen, W.E. Stewart, Chem. Engng. Sci. 22 (1967) 1483.
[125] B.A. Finlayson, The Method of Weighted Residuals and Variational Principle: With Applications in Fluid Mechanics, Heat and Mass Transfer, Academic Press, New York, 1972.
[126] J. Villadsen, M.L. Michelsen, Solution of Differential Equation Models by Polynomial Approximation, Prentice-Hall, Englewood Cliffs. NJ, 1978.
[127] J.P. Sörensen, W.E. Stewart, Chem. Engng. Sci. 37 (1982) 1103.
[128] L. Hosten, G.F. Froment, Ind. Engng. Chem. Proc. Des. Dev. 10 (1971) 280.
[129] G.B. Marin, G.F. Froment, Chem. Engng. Sci. 37 (1982) 759.
[130] P.A. Van Trimpont, G.B. Marin, G.F. Froment, Ind. Engng. Chem. Fund. 25 (1986) 544.
[131] P.A. Van Trimpont, G.B. Marin, G.F. Froment, Appl. Cat. 24 (1986) 53.
[132] P.A. Van Trimpont, G.B. Marin, G.F. Froment, Ind. Engng. Chem. Res. 27 (1988) 51.
[133] G.B. Marin, G.F. Froment, Proc. 1st Kuwait Conf. Hydrotreating Processes, EFCE Public. Ser. 27(II), 1989.
[134] L.L. Hegedus, C.J. Pereira, Chem. Engng. Sci. 45 (1990) 2027.